Tracking the invasion: dispersal of Hymenoscyphus fraxineus airborne inoculum at different scales

M Grosdidier, R. Ioos, C. Husson, O. Caël, T Scordia, Benoit Marçais

FEMS Microbiology Ecology, 94(5)
Accepted 21/02/2018
https://doi.org/10.1093/femsec/fiy049

Tracking the invasion: dispersal of *Hymenoscyphus fraxineus* airborne inoculum at different scales

Grosdidier M. [12*], Ioos R. [2], Husson C. [1], Cael O.[1], Scordia T. [3], Marçais B. [1]

*Corresponding Author: benoit.marçais@inra.fr

1 Université de Lorraine, Inra, IAM, F-54000 Nancy, France2 ANSES Laboratoire de la Santé des Végétaux, Unité de Mycologie, Domaine de Pixérécourt, Bâtiment E, F-54220 Malzéville, France

3 Département de la Santé des Forêts Auvergne-Rhône-Alpes, Ministère de l'agriculture et de l'alimentation DGAL-SDQPV, 251 rue de Vaugirard, F-75732, Paris cedex 15, France

Summary

Ash dieback is caused by an invasive pathogen, *Hymenoscyphus fraxineus,* which emerged in Europe in the 1990s and jeopardizes the management of ash stands. Although the biological cycle of the pathogen is well understood, its dispersal patterns via airborne spores remain poorly described. We investigated the seasonal and spatial patterns of dispersal in France using both a passive spore-trapping method coupled with a real-time PCR assay and reports of ash dieback based on symptom observations. Spores detection varies from year to year, with a detection ability of 30 to 47%, depending on meteorological conditions, which affect both production of inoculum and efficiency of the trapping. Nevertheless, our results are consistent and we showed that sporulation peak occurred from June to August and that spores were detected up to 50-100 km ahead of the disease front, proving the presence of the pathogen before any observation of symptoms. The spore dispersal gradient was steep, most of inoculum remaining within 50 m of infected ashes. Two dispersal kernels were fitted using Bayesian methods to estimate the mean dispersal distance of *H. fraxineus* from inoculum sources. The estimated mean distances of dispersal, either local or regional scale, were 1.4 km and 2.6 km, respectively, the best fitting kernel being the inverse power-law. This information may help to design disease management strategies.

Introduction

Forest ecosystems have been increasingly disturbed by emerging infectious diseases (EIDs) in the last few decades (Santini *et al.* 2013). Most of them are caused by fungal pathogens that affect forests in many ways, ranging from loss of biodiversity to altered environmental or economic services (Williams *et al.* 2010; Stenlid *et al.* 2011; Santini *et al.* 2013). EIDs may lead to growth reduction or severe mortality, and may drastically reduce local frequencies of species. To prevent their introduction, established regulations are based on lists of identified putative invasive organisms (Brasier 2008). However, basing the biosecurity measures on these lists may be unsatisfactory. Indeed, about 90% of fungal plant pathogens could remain undescribed (Crous and Groenewald 2005; Brasier 2008), and in addition, many invasive plant pathogens are described only after the start of the invasion process and can thus never be included in quarantine lists (Stenlid *et al.* 2011; Desprez-Loustau *et al.* 2016). Therefore, it appears impossible to prevent all introductions of new pathogens, stressing the importance of improving plant health surveillance to detect them as soon as possible after introduction as well as developing methods to limit their establishment.

One key to management of invasive pathogens is good knowledge about the dispersal patterns based on robust information on the pathogen distribution and on it means of dispersal. This information is strongly needed to develop strategies such as disease containment or eradication. Apple scab, Karnal bunt, Asian soybean rust and Sudden Oak Death are examples of EIDs for which management was greatly enhanced by this type of modeling (Aylor 1998; Stansbury *et al.* 2002; Pan *et al.* 2006; Cunniffe *et al.* 2016). Pathogenic fungi spreading by airborne inoculum are especially difficult to contain once they are established. In particular, knowledge about the long distance dispersal of the spores is usually lacking which hampers eradication and containment efforts (Rieux *et al.* 2014). Mathematical descriptions of dispersal patterns are often used to scale-up management actions (Bullock and Clarke 2000; Bullock, Shea and Skarpaas 2006; Devaux *et al.* 2006; Schurr, Steinitz and Nathan 2008; van Putten *et al.* 2012; Rieux *et al.* 2014). A probability density function (PDF) called a "dispersal

kernel" describes the distribution of post-dispersal destinations in relation to the location of the inoculum source. Dispersion can be modeled taking into account the direction of the inoculum, with anisotropic kernels using coordinates, or without any reference to direction, with isotropic kernels using only the distance between the source and the post-dispersal location (Nathan *et al.* 2012). Different kernel functions can be used based on the magnitude of the long-distance dispersal. Fat-tailed kernels such as exponential or power functions give more importance to long-distance dispersal than thin-tailed kernels, such as Gaussian and Student-t functions. The shape of the tail is crucial to describe the scale of dispersal and in particular to assess the importance of long distance dispersal (Clark *et al.* 1999).

Acquiring knowledge about fungal pathogen dispersal is essential, but the data are needed early during the invasion process in order to consider an efficient management. Trapping of airborne inoculum is a good way to infer the dispersal pattern without waiting several years to observe the realized disease dispersion (Peterson *et al.* 2015). Although traps coupled with real-time quantitative PCR have been frequently used to detect spores of fungal pathogens in affected area (Schweigkofler, O'Donnell and Garbelotto 2004; Ioos *et al.* 2009b; Chandelier, André and Laurent 2010; Ioos and Fourrier 2011; Luchi *et al.* 2013; Mahaffee and Stoll 2016), the ability of spore traps to detect invasive plant pathogens in area currently being invaded have seldom been tested (Jackson and Bayliss 2011). Two types of spore traps can be distinguished: passive traps such as wood-discs (Edman and Gustafsson 2003), Petri dishes (Gonthier *et al.* 2001) or Air-O-Cell (Jackson and Bayliss 2011), and active spore traps such as rotating-arm impaction devices (Chandelier *et al.* 2014) or Burkard samplers (Jackson and Bayliss 2011).. Active spore traps are more efficient but have several limitations: need for skilled staff, short battery life, sensitivity to particle size, and cost. They are therefore not appropriate to monitor the spread of a disease across a large area. Passive spore traps are less sensitive and more vulnerable to climatic conditions and damage, potentially leading to signal loss and reduced efficiency (Jackson and Bayliss 2011). However, passive spore traps have advantages for epidemiological monitoring and surveying: they are more adapted to large-scale studies because they are easily handled and less expensive.

Ash dieback is a good example of an EID induced by an alien pathogen that offers little possibility of control once established. The causal agent, *Hymenoscyphus fraxineus*, comes from Asia where it causes little damage to its original host, *Fraxinus mandshurica.* It emerged in the 1990s in Europe and has caused since severe dieback of *F. excelsior* and *F. angustifolia*. The pathogen was described late (Kowalski 2006) and identified as an invasive species only in 2011 (Husson *et al.* 2011; Queloz *et al.* 2011). In France, ash dieback was first observed in 2008 in the NE (Husson *et al.* 2011) and since then the progression of the disease has been carefully monitored by the French forest health survey (*Département de la Santé des Forêts,* DSF). This monitoring program provides essential information about dispersal processes. Unfortunately in France, information has been made available too late to consider an efficient containment of the disease. In addition, the high cost of the surveillance, from tree observation to sample collection and analysis, limits the amount of data collected. The disease is known to disperse at a regional scale by the movement of infected nursery stock and at a more local scale by the spread of efficient airborne fungal ascospores (Gross *et al.* 2014). Attempts to eradicate the disease have been implemented in some European countries, but with what appears to be an uncomplete success (McCracken *et al.* 2017). Eradication success indeed strongly depends on early detection and good knowledge about dispersal pattern to define the area that need to be treated (Cunniffe *et al.* 2016), data which are still lacking for *H. fraxineus*. Pathogen early detection coupled with good knowledge on dispersal pattern is therefore crucial for efficient disease management.

In this study, we thus assessed the ability of spore traps to detect *H. fraxineus* in area being invaded by the pathogen and to document its dispersal pattern at several spatial scales, from the vicinity of infected ashes to beyond the disease front. To achieve this goal, two methods of disease detection on the disease front were applied in parallel over four consecutive years. The first method is based on symptom observations and reports of ash dieback by the French surveillance system, and the second on a passive trapping system of wind-dispersed spores coupled with specific real-time PCR. Then, we assessed the importance of long distance dispersal using kernels with the aim to infer mean dispersal distance of the spores.

Material and Methods

National survey based on visual symptoms

The French forest health survey services (DSF, *Département de la Santé des Forêts*) has been reporting ash dieback symptoms for the country (crown dieback, canker shoots and collar canker) since the disease was first reported in eastern France in 2008. The survey has also reported the absence of symptoms (no visible shoot cankers or dieback) in many regions, and in particular those close to the disease front. Each DSF report contains information on the location and type of stand, date of observation, and confirmation of disease presence by laboratory analysis. Presence/absence of the disease is summarized by quadrat of 16 x 16 km (Nageleisen, Saintonge and Piou 2010; Boutte 2011). Based on these data, progression of the disease within France has been mapped (Figure 1, source: French forest health survey services).

Field experiments

Seasonal pattern of ascospore production. A first experiment aimed at studying seasonal patterns of *H. fraxineus* sporulation. Two sampling sites were set up in Gremecey and Seichamps (Nancy area, northeastern France) in two young ash stands strongly infected by *H. fraxineus* (Figure 1) where ash dieback was first reported in 2009. Trapping of *H. fraxineus* spores was carried out from 9 April 2010 to 16 March 2012. Six spore traps were set up in each of the stands (see below for the trapping protocol). In 2010, traps were exposed for between 6 to 48 days depending on the period of year (between 6 to 10 days before May, between 25 to 42 days from June to August, between 30 to 48 days from September to November 2011). In 2011 and 2012, traps were exposed for 15 days. In 2012, at the end of the trapping period, over 90% of ashes showed disease symptoms at both study sites.

Local pattern of dispersal. For the second experiment, a sampling area was established in order to determine the dispersal range of the pathogen at a local scale in Champenoux (northeastern France, Figure 1), where the disease was reported for the first time in 2009. The area was surveyed to determine the precise locations of individual ashes and the presence of *H. fraxineus* in plant tissue based on molecular testing (Ioos *et al.* 2009b). Traps were set up at distances ranging from 0 to 800 m from infected ashes and at locations evenly distributed across the sampling area (Figure 1). Spore traps were set up on 52 sites for three 15-day periods between early July and mid-August 2011. Afterwards, spore traps were set up at 124 sites in the last 15 days of July 2012, and at 130 sites during the first 15 days of July 2013, with an increased sampling effort at locations 600–800 m from infected ashes.

Regional-scale pattern of dispersal. In the third study, four sampling areas (SA I, II, III and IV) were installed in order to determine the *H. fraxineus* dispersal pattern at the regional scale (Figure 1). Sampling areas were selected based on progression of the disease in France. They were set up for two consecutive 15-day periods from mid-June to mid-July, every year from 2012 to 2015, in order to cover the disease front in central France (SA I and II), as well as in south-eastern France and the Rhone valley (SA III and IV). For SA III and IV, sites were also chosen on the basis of altitudinal and longitudinal gradients to take into account the temperature variabilities of the area. Potential sites were first defined for the presence of water courses and tree cover using Google Earth images before being visited, and only those with the presence of ashes were selected. One spore trap per site was set up close to the ashes (< 5 m) from mid-June to mid-July, taking into account the expected peak of sporulation. Forty-one sites were selected in 2012 (SA I), 100 in 2013 (SA II), 101 in 2014 (SA III), and 99 in 2015 (SA IV) (Figure 1).

Trapping method

Spore traps were designed based on a protocol modified from Schweigkofler, O'Donnell and Garbelotto (2004) as described in Grosdidier *et al.* (2017). Briefly, traps consisted of polystyrene blocks, placed 1 m above the ground with a 150 mm diameter no. 1 Whatman filter pinned to the top of the block (except for SA IV, where a no. 3 Whatman filter was used). The filter was sprayed with 4x TE buffer (40 mM Tris-HCl, 4 mM EDTA, pH 8.0) to prevent fungal spore germination. A negative control was introduced for each trap, in order to check the absence of contamination during the analysis process. The negative control was a filter enclosed hermetically in a plastic bag, and fixed to one side of each trap when the latter was installed and remained there all the trapping period long. Spore traps, including the negative control filters, were handled for sampling, washing, and DNA extraction according to Grosdidier *et al.* (2017).

During the DNA extraction step, four positive controls consisting of *H. fraxineus* spore solutions at 20 and 200 spores.μL^{-1} (each in duplicate) and four negative controls consisting of sterile water, were included during the DNA extraction steps as quality controls. In order to avoid analytical biases, individual filters from an annual sampling round were randomized before extraction and PCR.

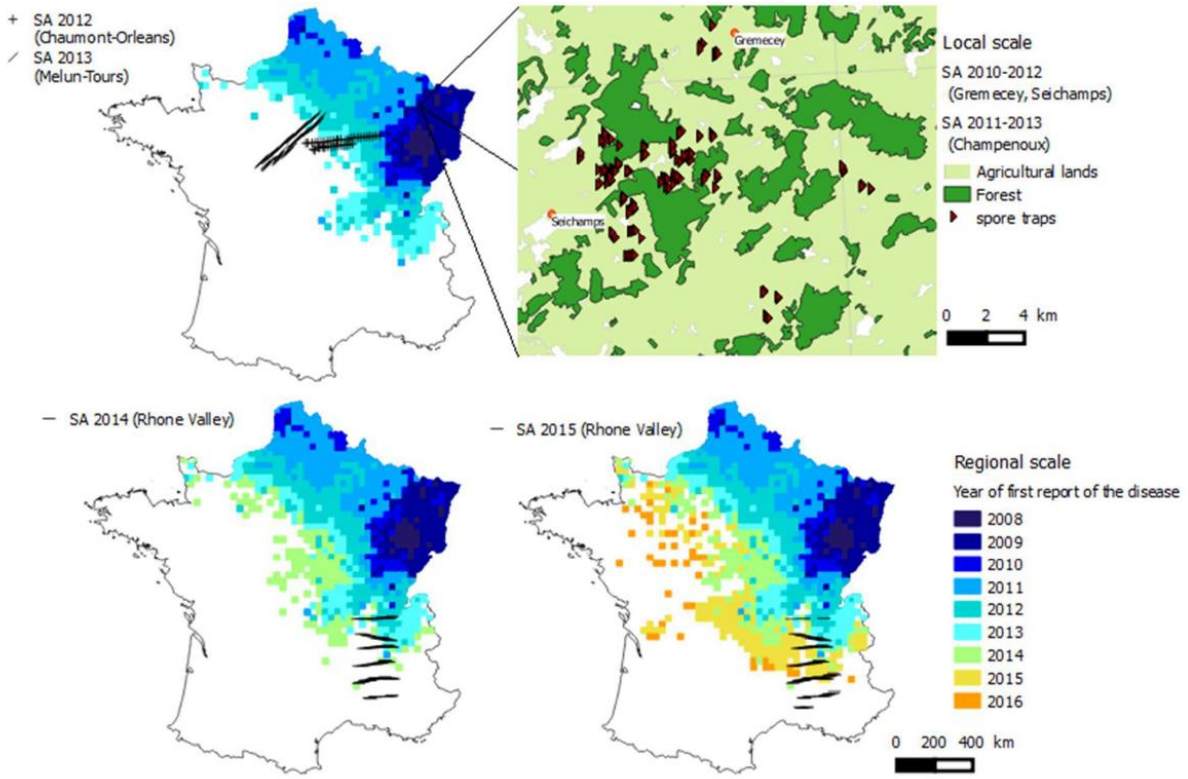

Figure 1: Maps of the disease progression in France based on symptoms observations with the sites of the sampling area at the local and regional scales. The colored graduations indicate the year of first ash dieback report in the quadrat by the DSF. At the local scale, traps were set up around Champenoux and Gremecey cities (France). At the regional scale, 41 sites were selected in 2012 in two transects between Chaumont (Marne) and Orleans (Loiret) (SA I: WGS84 NW-1.665 48.147 ; NE-5.023 48.118 ; SW-1.670 47.698 ; SE-5.000 47.669). In 2013, 100 sites were selected in two transects between Melun (Seine-et-Marne) and Tours (Indre-et-Loire) (SA II: WGS84 NW-0.304 48.581 ; NE-3.014 48.597 ; SW-0.352 47.323 ; SE-2.998 47.338). In 2014, 101 sites were selected in six transects across the Rhône River in the Rhône Valley south of Lyon (Rhône) (SA III: WGS84 NW-4.415 46.331 ; NE-5.712 46.300 ; SW-4.332 44.083 ; SE-5.579 44.053). In 2015, 99 sites were selected in seven transects across the Rhône River in the Rhône Valley south of Lyon (Rhône) (SA IV: WGS84 NW-4.430 45.934 ; NE-5.615 45.971 ; SW-4.732 44.078 ; SE-5.489 44.115).

Real-time PCR amplifications

Real-time PCR (qPCR) amplifications were performed according to Ioos *et al.* (2009a, 2009b), except that 45 cycles were performed for each run. DNA extracts were analyzed by qPCR with the Maxima Probe/ROX qPCR Master Mix (*Thermo Fisher Scientific*, Waltham, MA, USA) in three replicates for each filter included in different PCR runs, using an Agilent technologies Stratagene MX 3005 P thermal cycler (*Agilent Technologies*, Les Ulis, France) for all samples in the study, except samples from areas SA III and IV, for which a QuantStudio6 thermal cycler (*Life Technologies*, Saint-Aubin, France) was used. At least two non-template controls (NTCs, i.e. water) were included in each run. Different types of standard samples were used over the years. Calibrated *H. fraxineus* ascospore solutions were used for the sampling zones of the first and second experiments, whereas *H. fraxineus* genomic DNA was used for the I and II sampling zones, and plasmidic *H. fraxineus* target DNA for the SA III and IV sampling zones. These positive controls were systematically included in the analyses to build a standard curve. Results were quantified and analyzed as a number of spores.day^{-1}.m^{-2} or DNA ng.day^{-1}.m^{-2} or DNA copies.day^{-1}.m^{-2}. DNA quantities were transformed into number of spores using the positive control values.

Grosdidier *et al.* (2017) demonstrated that DNA samples generating Ct values below 45 after the *H. fraxineus*-specific PCR we used in this study (Ioos *et al.* 2009a, 2009b) can be reliably rated as positive. Four amplicons generated from DNA extracts of filter exposed in SA III and associated to late Ct values (40-45) were sequenced. The analysis of the sequences confirmed that the amplified DNA did correspond to *H. fraxineus* target DNA (Grosdidier *et al.* 2017). Moreover, Husson *et al.* (2011) showed that this *H. fraxineus*-specific PCR does not cross with DNA of the closely related and widespread endophyte *Hymenoscyphus albidus*. A filter was considered positive if at least two replicates out of three yielded a Ct value. A site was considered positive when at least one filter out of all filters set on-site during the periods (one, two or three) was positive after qPCR analysis.

Trapping method vs. reports of ash dieback

For SA I, II, III and IV, results of trapping were compared to observations of symptoms by the forest health survey system (DSF). The vicinity of a trap was chosen as a 24-km radius circle around the trap. This value was selected from the outset to match the radius of a 16 x 16 km DSF quadrat and its adjacent quadrats (3 x 16 / 2). For each sampling area, traps were separated in four categories according to *H. fraxineus* DNA detection and reports of ash dieback symptoms by the DSF in the vicinity: A, detection of *H. fraxineus* DNA on the trap (D+) and report of ash dieback in the vicinity (R+); B, detection of *H. fraxineus* DNA on the trap (D+) but no report of the disease in the vicinity (R-); C, no detection of *H. fraxineus* DNA on the trap (D-) but report of ash dieback in the trap vicinity (R+); and D, both negative (D-R-). The frequency of each category (A, B, C and D) was computed.

Then, to compare the two methods of *H. fraxineus* detection, the reports of ash dieback by the DSF in the vicinity of the traps were taken into account during the year of trapping and also in the two following years. A first binomial generalized linear model (GLM) analysis was carried out using *H. fraxineus* detection by traps as the response variable. The year of trapping, which also corresponds to a sampling area (one year = one area), and number of years of ash dieback presence in the area were set as the explicative variables. The likelihood of traps detecting *H. fraxineus* spores in the vicinity of positive DSF reports, depending on the number of years of disease presence and sampling area was quantified with an odds ratio (1), estimated as the exponential of the coefficient parameter “number of years of disease presence”. A second binomial generalized linear model analysis was carried out using the presence of a DSF report in the vicinity of traps as the response variable according to trap detection, and the number of years between the trapping and the report of ash dieback presence by the DSF. Only traps located more than 50 km ahead of the disease front were selected for this analysis; this was done to avoid the bias that could arise from disease dispersal, which is about 50 km per year. The likelihood of observing DSF reports of ash dieback in the vicinity of traps detecting *H. fraxineus* one or two years after the trapping was quantified with an odds ratio (2).

Construction of dispersal models

Z_i, the number of spores detected on a filter (spore.m^{-2}.day^{-1}), is modeled by a zero-inflated negative binomial. For the local scale, each period of trapping was used individually, but for the regional scale, an average between two periods of trapping was computed. The underlying hypothesis is that data result from two successive phenomena: first, the likelihood of spore detection was modeled by a Bernoulli distribution with parameter p characterizing the rate of detection (1-p) ; and second, Z was modeled by a negative binomial distribution with parameter k characterizing the over-dispersion. The model can be written as:

$$Z_i \sim Negative\ Binomial(\mu_i, k_i) \text{ where } \mu_i = \frac{k}{s_i + k} \text{ and } s_i = (1 - u_i) * \lambda_i$$

$$u_i \sim Bernouilli\ (p)$$

$$\text{where } \lambda_i = \exp(\partial_1(i) + \partial_2(i) + d_i * F_i) \quad \text{for the local scale and}$$

$$\lambda_i = \exp(\partial_1(i) + d_i * F_i) \text{ for the regional scale}$$

where ∂_1 is a period random factor N(0,σ_1^2) (year for the regional scale and period nested in the year for the local scale), and ∂_2 is a site random factor N(0,σ_2^2). μ_i is the success probability of negative binomial. 1-p is the *H. fraxineus* detection efficiency (likelihood of detection by the trap close to the inoculum source). d_i is either the isotropic dispersal kernel with dispersal parameters a and b at distance r_i between sites i of traps and infected ash at the local scale, or the anisotropic two-dimensional dispersal location kernel at distance $rdist_i$ between sites i of traps set up and the nearest report of ash dieback by the DSF in the vicinity. Two different kernels used in dispersal studies (Clark *et al.* 1999; Bullock and Clarke 2000; Clark *et al.* 2005; Bullock, Shea and Skarpaas 2006; Nathan *et al.* 2012) were tested. They were selected according to the type of tail and scales observed. The first kernel is Gaussian distribution corresponding to a concave curve near to the source with a thin-tail. It is used for dispersal through diffusion or completely random walk. The second kernel is inverse power-law distribution used for long-distance pollen dispersal with a convex curve near to the source and very fat-tail. Dispersal distance kernels were used for the local scale analysis using the equations of (Nathan *et al.* 2012). Two-dimensional dispersal location kernels were used for the regional scale analysis using the equations of (Nathan *et al.* 2012), modified according to (van Putten *et al.* 2012) to remove any directional effect (*i.e.* π or 2π) (Table 1).

$$rdist(X_i, Y_i) = \sqrt{(2\gamma^2 + 1)\left(\frac{{X_i}^2}{\beta^2} + \frac{2\gamma X_i}{\beta}\right) + (\gamma^2 + 1)({Y_i}^2 + 2\gamma^2) - 2\gamma\left(\frac{X_i}{\beta} + \gamma\right)\sqrt{(\gamma^2 + 1)\left(\left(\frac{X_i}{\beta} + \gamma\right)^2 + {Y_i}^2 + 1\right)}}$$

$$Y_i = (x_i - {x_i}^*)\sin\psi_i - (y_i - {y_i}^*)\cos\psi_i$$

$$X_i = (x_i - x_i^*)\cos\psi_i + (y_i - y_i^*)\sin\psi_i$$

Where x_i and y_i, are coordinates of the trap, x_i^* and y_i^* are coordinates of the ash dieback observation by the DSF, ψ_i, rotation parameter (-π < ψ_i ≤ π) which describes the angle between lines joining traps and ash dieback DSF reports and the north. β is the coherency parameter ($\beta > 0$) which represents flattening along a common axis and shapes spore shadow oval. γ is the drift parameter ($\gamma \geq 0$) which represents the strength of the directional effect. F_i equals 1 for the isotropic dispersal kernel or equals $\frac{\left(\frac{1}{2*\pi*\beta*\sqrt{\gamma^2+1}}\right)}{rdist_i}$ for the anisotropic dispersal kernel.

The models were fitted into a Bayesian frame using three Markov chain Monte Carlo (MCMC) methods and assessing convergence with a Gelman-Rubin test. Non-informative priors were chosen for all model parameters, a gamma distribution G(0.001,0.001) for variance of random effect ∂_1 and ∂_2, a uniform distribution U(0,100) for k, the over-dispersion parameter of the negative binomial distribution, a gamma distribution G(2,0.01) for the scale parameter a (according to (Chung *et al.* 2013), a gamma distribution G(2,1) truncated (2,100) for the shape parameter b, a uniform distribution U(0.1,3) for coherency parameter β, a uniform distribution U(0,1) for drift parameter γ, and a beta distribution U(1,1) for parameter p of Bernoulli distribution. 1000 iterations with a burning period of 1000 iterations and 200 thin were required to reach convergence. Models were first tested with an intercept. However, as an intercept induced identifiability problems, it was removed in the last step to simplify the models.

Mean dispersal distance represents the average distance that an ascospore travels from an infected ash before reaching a trap. This was computed as $\frac{a\sqrt{\pi}}{2}$ for the Gaussian distance kernel and as $\frac{2a}{b-3}$ for the inverse power-law distance kernel, with a the scale parameter and b the shape parameter (Nathan *et al.* 2012), and as the scale parameter a for location kernels.

Table 1: Functional forms of the kernels distributions tested according to the two types of kernels. Scale parameter a is higher than zero and shape parameter b is higher than two.

	Isotropic distance kernel	Anisotropic location kernel
Gaussian (thin-tail)	$d_g(a,r) = \frac{1}{\pi a^2} * \exp\left(-\frac{r^2}{a^2}\right)$	$d_g(a,rdist) = \frac{1}{a^2} * \exp\left(-\frac{rdist^2}{a^2}\right)$
Inverse power-law (fat-tail)	$d_{ip}(a,b,r) = \frac{(b-1)*(b-2)}{2\pi a^2} * \left(1+\frac{r}{a}\right)^{-b}$	$d_{ip}(a,b,rdist) = \frac{(b-1)*(b-2)}{a^2} * \left(1+\frac{rdist}{a}\right)^{-b}$

Results

Sporulation and dispersal patterns at the local scale

Overall, the traps detected *H. fraxineus* spores in a range of 2 – 2560 spores.day^{-1}.m^{-2} across all trapping experiments and years.

Seasonal pattern of ascospore production. Airborne inoculum was detected only during the late spring and summer both in 2010 and 2011. In 2010, sporulation peak was observed in late July while in 2011, it was observed in late June (in both cases > 1000 spores.day^{-1}.m^{-2}, Figure 2). The quantities of spores caught by the trapping method were not significantly different at Grémecey and at Seichamps (Wilcoxon test *p*-value = 0.93). Airborne inoculum was detected in abundance by the trapping method for a short period between late June and late July. Based on the first year results, an exposure period of 15 days was a good compromise to capture a sufficient amount of spore to be detected. For the subsequent experiments, trapping was set up during this favorable period with a time exposure of 15 days.

Local pattern of dispersal. The frequency of detection of *H. fraxineus* by traps and the number of spores detected were maximum under the infected ashes (distance of 0 m from the inoculum source). No *H. fraxineus* inocula were detected by traps further than 500 m from infected ashes. Inoculum density decreased rapidly up to 50 m from infected ashes and remained at a low level up to 500 m (<20 spores.day^{-1}.m^{-2}) (Figure 3). The inverse power-law kernel fitted the data slightly better than the Gaussian kernel (deviance information criterion (DIC) of 826.3 and 848.6, respectively) (Table 2). The detection efficiency by traps (1-p) was low at 0.47 (CI [0.31–0.67]). The two random effects ∂_1 and ∂_2 induced some variability with variances σ^2_1 equal to 2.05 (CI [0.78–84.42]) and σ^2_2 equal to 18.22 (CI [12.13–39.58]). The mean dispersal distance inferred was 173 m (CI [12–420]) for the Gaussian kernel, and 1375 m (CI [64–3324]) for the inverse power-law kernel. Parameter k was estimated at 1.13 (CI [0.25–2.06]), which indicated significant over-dispersion of the data.

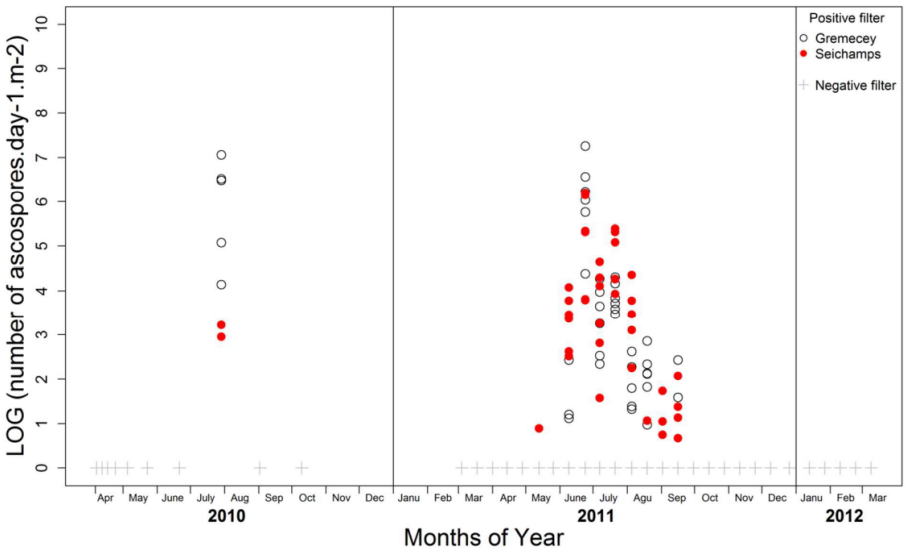

Figure 2: Logarithm of the quantities of ascospores of *H. fraxineus* detected by the traps per day and per m^2 according to the period of trapping, the year and the site.

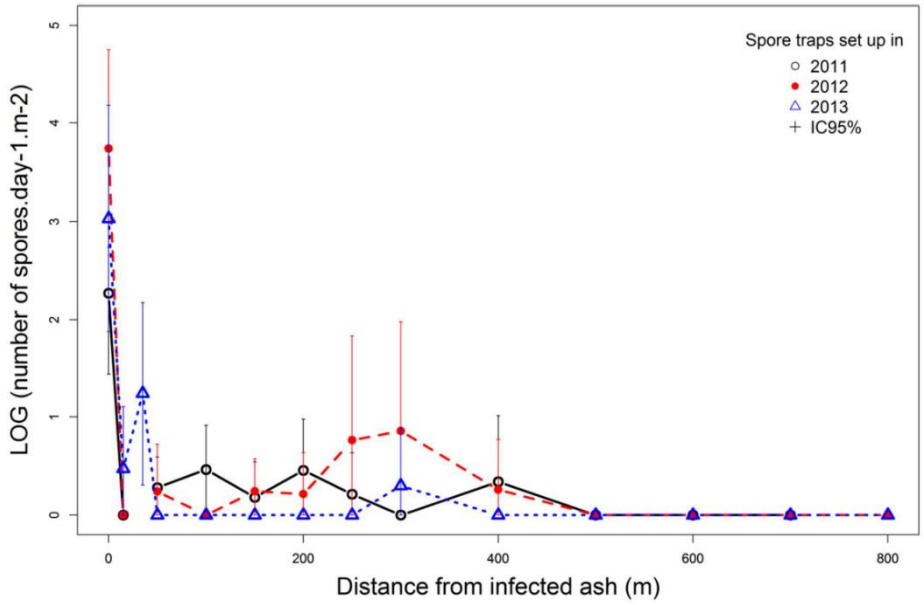

Figure 3: Logarithm of the quantities of ascospores of *H. fraxineus* detected by the traps per day and per m^2 according to the distance from the infected ash and the year where the trap are set up (local scale).

At the regional scale: spore traps vs. DSF reports of symptoms

Results of trapping

The frequency of *H. fraxineus* DNA detection on filters depended on the year of sampling with 39% of traps at SA I in 2012, 7% of traps at SA II in 2013, 34% of traps at SA III in 2014, and 10% of traps at SA IV in 2015. The 341 negative controls filters attached with all exposed filters, yielded negative results, as expected.

Dispersal pattern

At the regional scale (SA I to IV), we studied the relationship between detection of *H. fraxineus* on traps and local reports of ash dieback by the DSF. *H. fraxineus* inoculum was detected by the traps in locations where the nearest DSF report of ash dieback was observed 38 km away in 2012, 116 km in 2013, 56 km in 2014, and 13 km in 2015. The number of spores detected on the traps decreased rapidly with increasing distance from a DSF ash dieback report and stabilized between 5 and 20 km (Figure 4a). At more than 20 km from a DSF ash dieback report, the average quantity of spores trapped was very low at about 4 $spores.day^{-1}.m^{-2}$. For traps located close to DSF ash dieback reports (< 20–25 km), no anisotropy could be observed, with no preferential direction between the trap and the ash dieback report. However, for traps located far away (> 25 km) from the nearest ash dieback DSF report, clear anisotropy could be observed with preferential spread of the disease at long distances toward the south-west in 2012–13 and the south in 2014–15 (Figure 4b). At the regional scale, we thus tested anisotropic kernels to analyze the dispersal pattern of *H. fraxineus*. The deviance information criterion (DIC) for the Gaussian kernel was higher than for the inverse power-law kernel (923.6 versus 911.2), although the difference remained limited. The efficiency of *H. fraxineus* detection by the traps (1-p) was 0.30 (CI [0.17–0.59]). The year random effect induced some variability with a variance σ_2^2 of 10.71 (CI [3.84–1111.4]). The mean distance between a trap detecting *H. fraxineus* and a DSF ash dieback report was 590 m (CI [180–1330]) for the Gaussian kernel, and 2560 m (CI [80–7650]) for the inverse power-law kernel. A south-west directionality was observed with coherency parameter β and drift parameter γ higher than 0 (1.28 and 0.35, respectively). The value of parameter k was estimated at 0.32, which meant that the level of over-dispersion in the data was low.

Probabilities of visual disease detection and detection by the trapping method

Altogether, 57 traps out of 341 (16.7%) detected *H. fraxineus* when ash dieback was reported by the DSF within 24 km, and 149 out of 341 (43.7%) did not detect *H. fraxineus* when no ash dieback was reported by the DSF within 24 km. Therefore, for 60% of the traps, trapping results were in agreement with disease symptom reports by the DSF. Conversely, 2.9% detected *H. fraxineus* while no ash dieback was reported by the DSF within 24 km. Finally, 36.4% did not detect *H. fraxineus* although ash dieback was reported by the DSF within 24 km (i.e. in *H. fraxineus* infected-areas) (Figure 5). About 25% to 30% of the traps were in this last category in the years 2012–14, while 65% of the traps were in this category in 2015 (Figure 5).

The probability of detecting *H. fraxineus* inoculum by the trapping method also depended on the duration of disease presence in the area (Figure 6). Fewer than 10% of the traps detected spores in areas where the disease had not yet been reported (closest DSF ash dieback report at more than 24 km away). This proportion increased with the number of years of disease presence, although not at the same rate in the different years of sampling. The decrease in 2012 at least two years before disease arrival is caused by the very little sampling effort (only two traps in this category). A logistic regression model was used to explain the proportion of traps detecting *H. fraxineus* spores, depending on the number of years of disease presence and sampling area, which also encompassed the year effect and indirectly climate. The probability of detecting the fungus by the trapping method increased with the number of years of disease presence (*p*-values < 0.01), with an odds ratio (1) of 3.5 (CI [2.32–4.79]) per year.

Table 2: Deviance Information Criterion and parameters of the dispersal models adjusted at local and regional scales.

Scale	Local scale		Regional scale	
Kernel distribution	Gaussian Isotropic distance kernel (thin-tail)	Inverse Power-law Isotropic distance kernel (fat-tail)	Gaussian Anisotropic location kernel (thin-tail)	Inverse Power-law Anisotropic location kernel (fat-tail)
DIC	848.6	826.3	923.6	911.2
Parameters [a]	Mean [IC 95%]	Mean [IC 95%]	Mean [IC 95%]	Mean [IC 95%]
σ_1^2	2.03 [0.75-110.5]	2.08 [0.80-58.34]	9.86 [3.58-657.89]	11.57 [4.11-1564.94]
σ_2^2	17.68 [12.06-40.65]	18.76 [12.21-38.52]	/	/
a	195.62 [13.13-473.74]	206.26 [9.67-498.6]	0.59 [0.18-1.33]	2.56 [0.08-7.65]
b	/	3.30 [2.00-5.67]	/	5.56 [2.50-9.39]
Pr	0.53 [0.31-0.69]	0.53 [0.35-0.69]	0.69 [0.37-0.83]	0.71 [0.45-0.84]
k	1.13 [0.27-2.09]	1.13 [0.23-2.02]	0.31 [0.03-0.54]	0.33 [0.04-0.57]
γ	/	/	0.35 [0.10-0.54]	0.34 [0.06-0.54]
β	/	/	1.28 [0.37-2.58]	1.28 [0.20-2.54]
Mean dispersal distance (km)[b]	0.17 [0.01-0.42]	1.38 [0.64-3.32]	0.59 [0.18-1.33]	2.56 [0.08-7.65]

[a] The Gelman-Rubin test indicated convergence for all reported parameters (Rhat very close to 1).

[b] For Anisotropic kernel, mean dispersal distance of $\frac{a\sqrt{\pi}}{2}$ for the Gaussian distance kernel and of $\frac{2a}{b-3}$ for the inverse power-law distance kernel. For isotropic kernels, mean dispersal distance is given by parameter a. Result is converted in km.

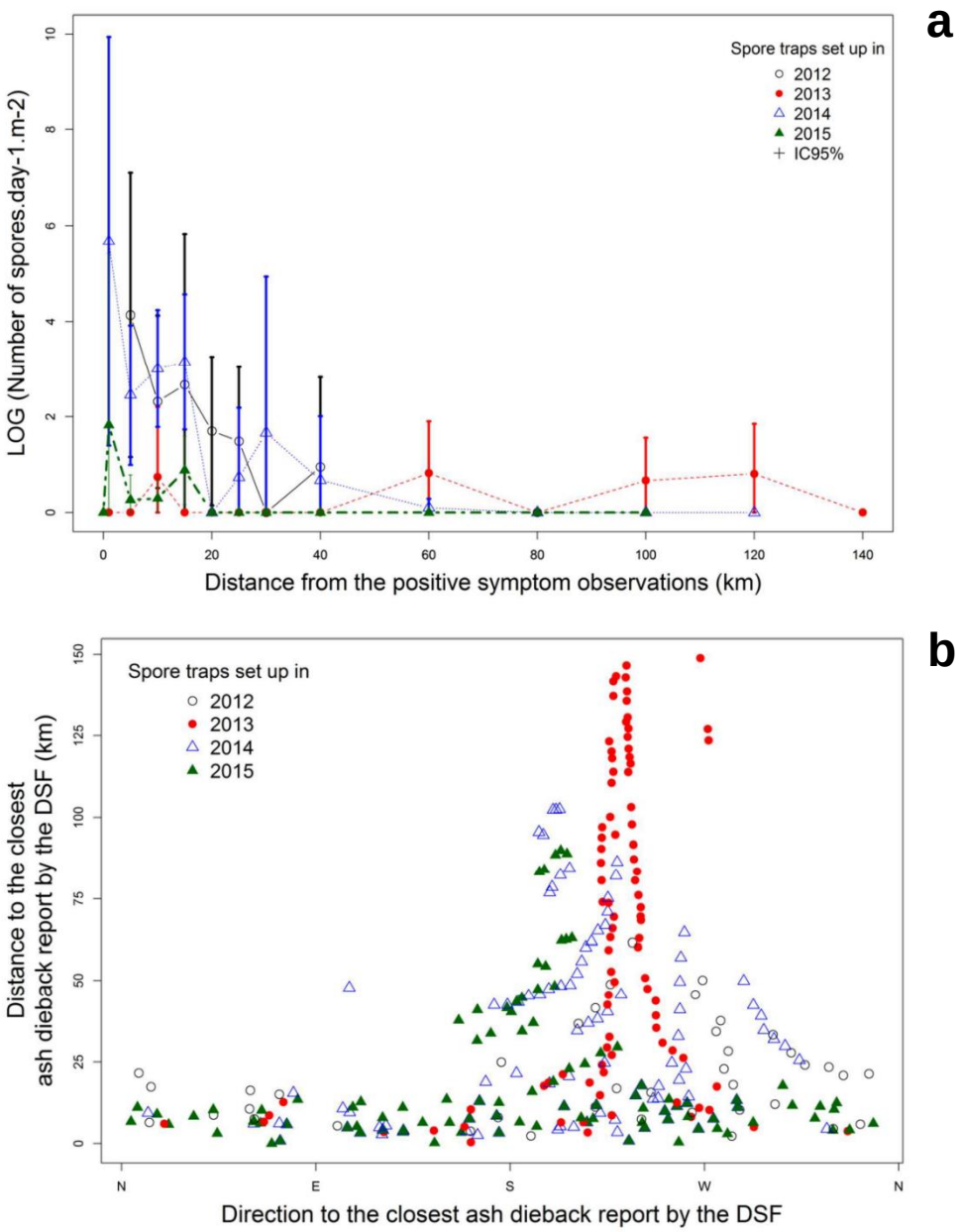

Figure 4: *Hymenoscyphus fraxineus* detected by the traps according to the distance from the nearest ash dieback report by the DSF. *a*) Quantities of spores of *H. fraxineus* caught by the traps per day and per m^2. *b*) Anisotropy in long distance dispersal of *H. fraxineus* ascospores.

The ability of trapping to predict future reports of ash dieback by the DSF in the area was also investigated. To this end, traps within 50 km of the disease front, i.e. average annual progression of the disease, were omitted (all traps set up in 2012, for example). We observed that all traps detecting *H. fraxineus* while no ash dieback was reported by the DSF within 24 km in the year of the trapping were associated with an ash dieback report in the vicinity within the following three years. The likelihood of a DSF ash dieback report in the vicinity one to three years after trap setting was significantly higher for traps which detected *H. fraxineus* than for traps which did not (Table 3). The interaction between *H. fraxineus* detection by traps and the number of years after trap setting was not significant (*p*-value > 0.99). As a result, a single odds ratio (2) of 8.6 (CI [3.23–26.3]) could be computed for an increased likelihood of a DSF report when the trap detected *H. fraxineus*.

Table 3: Probability to have at least one observation of disease symptoms in the neighborhood of traps zero, one, two, or three years after trap setting according to the transect and to the detection of *H. fraxineus* by qPCR the year of trap setting.

Number of years after trap are set	Sampling area	Probability to have at least one report of ash dieback by the DSF in the trap neighborhood (less than 24 km)	
		H. fraxineus positive filter traps	*H. fraxineus* negative filter traps
1	IV 2013	0,5	0,20
	V-A 2014	1	0,20
	V-B 2015	no trap	0
2	IV 2013	1	0,84
	V-A 2014	1	0.20
	V-B 2015	no trap	no trap
3	IV 2013	1	1
	V-A 2014	/	/
	V-B 2015	no trap	no trap

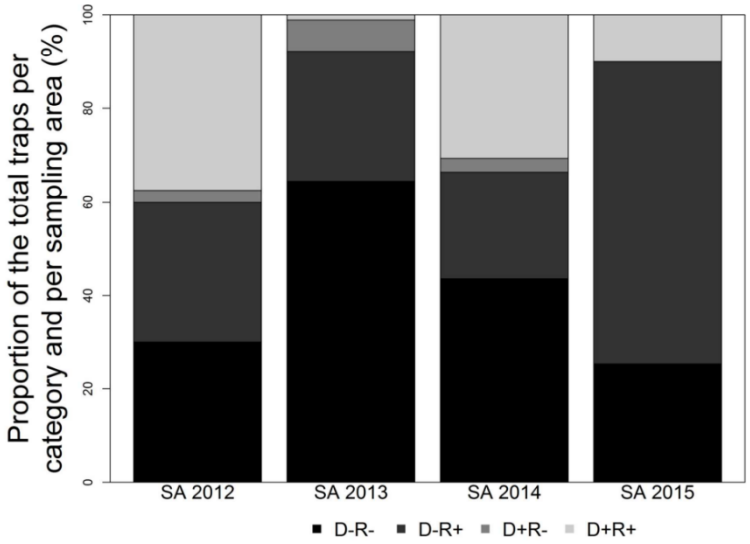

Figure 5: Proportion of traps according to the categories (A, B, C and D) and the sampling area the year of trap are setting. Categories are detailed with D+ detection of *H. fraxineus* by the trap, R+, report of ash dieback by DSF within 24km, D- and R- no detection of *H. fraxineus* by the trap or report of ash dieback by DSF within 24km.

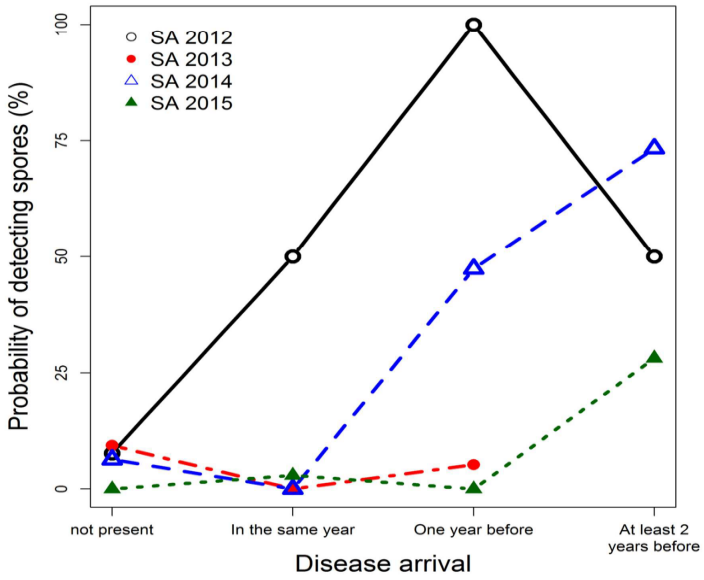

Figure 6: Probability of *H. fraxineus* spores detection by the trapping method according to the time of disease presence and the sampling area. The decreased observed for year 2012 and for at least 2 years of disease presence concerned a very low number of traps (N = 2) and will not be interpreted.

Discussion

This study described the dispersal pattern of *Hymenoscyphus fraxineus* at several scales. We showed that although the spore traps used have relatively low detection efficiency (0.3 to 0.5), they can track the pathogen presence in area being invaded and provide useful information such as *H. fraxineus* presence up to 100 km ahead of the disease front. The inverse power-law kernel analysis showed that *H. fraxineus* spores spread at an average distance of 1.4–2.6 km from an inoculum source. The level of detection confirms that the spore-trapping method could be used in addition to observations of disease symptoms on hosts in disease surveillance systems.

Low efficiency of passive traps has been emphasized in the literature (Jackson and Bayliss 2011) and this observation was confirmed by our results. Indeed, the parameter of the binomial component of the zero-inflated negative binomial measures the detection likelihood at the inoculum source, close to infected ashes. It characterizes the overall efficiency of the traps in detecting *H. fraxineus,* which ranged from 0.3 to 0.47 depending on the experiments. In fact, *H. fraxineus* apothecia were observed at some of the sites where traps did not detect the pathogen spores. Another possible cause of this low detection efficiency could be the long period of filter exposure; we chose to expose the filters for 15 days in order to maximize the chances of encompassing sporulation events and to better integrate weather variability. However, spiking filters with known amounts of *H. fraxineus* spores before exposure has shown that a large part of the signal may be lost during the trapping process by washout during rain events (*Husson,* personal communication) or other adverse weather conditions such as dry periods or wind. The addition of sticky substances, such as petroleum jelly, may improve trapping efficiency by limiting this washout during rain events (Jackson and Bayliss 2011; Dvorak, Rotkova and Botella 2016); preliminary tests showed that adding 5 ml petroleum jelly on the surface of 150 mm Whatman filter improved the efficiency of our traps (DNA quantities recovered three times higher, M. Grosdidier, unpublished results) and this procedure is now implemented routinely. Finally, the timing of sampling could also be crucial for the efficiency of trapping. The spore-trapping method requires knowledge of when sporulation peak occurs in order to maximize the chances of pathogen detection. The sporulation period in the north-east of France was found to be a short period between mid-June and mid-August, with sporulation peak in late June and early July. These results only partly match findings reported in the literature. Interestingly, most of the aerial *H. fraxineus* inoculum measured in the Czech Republic, in Norway, or in Belgium (close to north-eastern France), was detected in July and August (*Chandelier et al.*, 2014; *Dvorak et al.*, 2016; *Hietala et al.*, 2013; *Timmermann et al*., 2011). These authors did not observe the same defined peak in sporulation that we found in France, but rather a sporulation period that was more spread out over July and August. We also observed that the timing and intensity of the *H. fraxineus* sporulation peak varied across years and sites. This variability suggests that sporulation events are climate-dependent, which was already reported by Chandelier *et al.* (2014). Extreme climate events may be critical for trapping efficiency: during summer 2015, lower overall trapping efficiency may be explained by the heat wave that occurred in the area during the trapping period, with mean temperatures up to 3.5°C higher than mean *1981–2010* summer temperatures (Météo-France). Kowalski and

Bartnik (2012) showed very limited growth of *H. fraxineus* at 30°C and Hauptman *et al.* (2013) confirmed that temperatures higher than 30°C negatively affects the fungus survival in host tissues. During the period of trapping in 2015, the maximum daily temperature commonly reached these extreme values and could have led to decreased production of apothecia and ascospores. Also, in 2013, dispersal pattern in SA II shows few detection in the first kilometers, closed to the inoculum source, unlike others patterns. First, sampling effort close to infected ashes was less important than others SA. Then, during the period of trapping, severe thunderstorms were taking place in this SA II. These extreme events may transport spores far away (up to 100 km) and washout with the rain spores that had falling in the storm area. This possible impact of climate on the trapping was taken into account in the analysis by the period random factor (∂_1) that indeed induced in all case a significant variability. The site random factor (∂_2) that accounts for uncertainty regarding the extent of the local inoculum source and conduciveness of the site environment to sporulation was also a significant variability source.

Despite low spore detection by the traps and possible incomplete reporting of ash dieback symptoms by the DSF, this study provides valuable information on the *H. fraxineus* dispersal range. Because of the asymmetric posterior distribution, the accuracy of several model parameters remained low, particularly on the mean dispersal distance. Depending on the scale and the kernel considered, the mean dispersal distance was estimated at 0.2 to 2.6 km. The main cause of variability came from the kernel used, with a value about 3 times higher for the inverse power-law kernel, compared to the Gaussian kernel. The four models tested did not lead to clear-cut conclusions about the shape of the dispersal kernel, although the fat-tail kernel used (inverse power-law) fitted the data slightly better than the thin-tail kernel (Gaussian) at both the local and regional scales. This better fit of the fat-tail kernel reflects that although the amount of spores far dispersed is low, it remains substantial at large distances from the infected source, which explains the detection of spore up to 100 km from source at the regional scale. These detection far from any known inoculum sources have been verified by sequencing the PCR amplicon obtained with DNA from the traps (Grosdidier *et al.* 2017). Moreover, the likelihood of detecting the pathogen although no *H. fraxineus* is present was shown to be only 0.015% for this trapping method (Grosdidier *et al.* 2017). The sampling effort at large distances from infected ashes at the regional scale was far greater than at local scale, which might explain that we detect more long distance dispersal event at that scale. Alternatively, turbulence diffusion of airborne spores has been reported to be more efficient at larger scales which could explain this result (Scherm, 1996). Altogether, the mean dispersal distance given by the Inverse power law at local and regional scale was similar (0.6–3.3 versus 0.1–7.7). Part of the variability could be explained by the high variances of random factors (trapping period and site) that impact posterior distribution of model parameters asymmetrically. The analysis of *H. fraxineus* also showed that the over-dispersion parameter of the negative binomial law was significantly above 1, at the local scale but not at the regional scale. One explanation could be that anisotropy was not considered at the local scale; also, variability may be exacerbated when a finer scale is considered.

At the local scale, most of the spores fall very close to their source. The decrease in spore load in the air in the first 50 m from an inoculum source is very sharp, which is in agreement with the findings reported by Chandelier *et al.* (2014), even though *H. fraxineus* spores can be detected by traps up to 500 m from infected ashes. Local wind that could be associated with turbulence at the local scale could transport *H. fraxineus* spores to several hundred meters from infected ashes. If spores are released during turbulence, they could be lifted above the tree canopy and transported long distances from infected ashes. This phenomenon may be significant for spore size less than 10 µm, which is in the range of *H. fraxineus* ascospores (13–21 x 3–5 µm) (Gross *et al.* 2014; Norros *et al.* 2014).

At the regional scale, the amount of spores decreases quickly within 20–30 km from a positive DSF report. This brings some support to our presumptive choice based on the DSF quadrat size of a neighborhood of 24 km for the analysis. Long-distance dispersal of spores is nevertheless observed up to about 100 km ahead of the disease front. This limited amount of far-dispersed ascospores is not necessarily associated with establishment and creation of new disease foci. This may depend on the local environment (host densities and site conditions), but also the possibility for the pathogen to sexually reproduce. *H. fraxineus* is heterothallic and thus requires the encounter of the 2 mating types to produce apothecia and inoculum, which may not be possible if infection is too sparse. When these long-distance dispersed ascospores establish a disease focus, they may have a disproportionate effect on disease spread. The speed of ash dieback spread has been estimated, either at the European scale or in a single country, to be roughly in the range of 40 – 75 km (Gross 2013; Luchi *et al.* 2013; Laiviņš, Priede and Pušpure 2016). Therefore, the disease dispersal speed observed in Europe matches the range of long-distance dispersal events that we observed in France. Our study further shows that a delay of one to two years may occur between the arrival of spores on leaves from long-distance dispersal and the first report of ash dieback by the surveillance system. As disease symptoms reported by the DSF relate to shoot symptoms, at least one year is necessary for the transition from leaf infection induced by spores to shoot infections.

Modeling the *H. fraxineus* dispersal gradient from a source of inoculum showed that most of the inoculum remains close to the infected ash. This information could be used to develop management strategies. For example, attempts at eradication have been made in some countries, such as Ireland (McCracken *et al.* 2017), and our study provided data to define the size of the area that needs to be treated. The trapping system may also help to better take local conditions into account. Skovsgaard *et al.* (2017) explained that forestry actions need to be adapted to each site. The inferred distances of dispersal suggest that removing ashes within a radius of 1–2 kilometers of a focus, which is already very ambitious, would not be very effective as the mean spore dispersal distance is in that range. At best it would limit local inoculum production and might slow further disease spread. This has been studied theoretically by modelling for sudden oak death in California (Cunniffe *et al.* 2016), where, although pathogen has spread beyond the point where eradication is possible, containment of the disease may still be an option. These authors used a model to explore management strategies to limit the disease spread by determining how local treatment would be best deployed, and which areas could be the best targeted for eradication. Modeling pathogen dispersal patterns may help in designing control strategies by identifying key parameters of pathogen dispersal, by identifying inoculum reservoirs and dispersal corridors that foster the spread of infective propagules (Meentemeyer *et al.* 2011).

Early detection of a disease is also a critical part of the process. If a disease is detected after several years, it may have developed to the point of becoming impossible to eradicate. For example, when ash dieback was first reported in 2008 in France, in Haute-Saône, the prevalence and extent of disease were already very high over a large area. It is very likely that ash dieback had been present there for several years. Had a cost-effective spore-trapping system been set up at that time, the disease might have been detected earlier, for example in nurseries before out planting of the infected seedlings, and possible early eradication measures taken. Moreover, a DNA archive would have been available and could have been used subsequently to provide critical information about the initial pathogen presence in France and its possible route of introduction. Nevertheless, the trapping method will not replace symptom observations by qualified professionals working as part of the plant health surveillance system, and forest management close to the disease front is always difficult. Cunniffe *et al.* (2016) explained that applying a tradeoff between probability of detection (prevention of spread by early detection) and deployment of earlier treatment on selecting sites help to maximize the cost-effectiveness of management strategy.

Acknowledgements

We greatly appreciate the technical support of Anne Chandelier and the valuable assistance provided by Anaïs Gillet, and Emilie Hoscheit. This work was supported by grants from the Forestry Health Department, French Ministry of Agriculture and Forestry, ANSES, and the Biodiversa EU project RESIPATH. The UMR1136 research unit is supported by a grant managed by the French National Research Agency (ANR) as part of the "*Investissements d'Avenir*" program (ANR-11-LABX-0002-01, Laboratory of Excellence ARBRE).

References

Aylor DE. The Aerobiology of Apple Scab. *Plant Dis* 1998;**82**:838–49.

Boutte B. Les réseaux d'observation du Département de la Santé des forêts. *forêt méditerranéenne* 2011;**XXXII**:119–26.

Brasier CM. The biosecurity threat to the UK and global environment from international trade in plants. *Plant Pathol* 2008;**57**:792–808.

Bullock JM, Clarke RT. Long distance seed dispersal by wind: measuring and modelling the tail of the curve. *Oecologia* 2000;**124**:506–21.

Bullock JM, Shea K, Skarpaas O. Measuring plant dispersal: an introduction to field methods and experimental design. *Plant Ecol* 2006;**186**:217–34.

Chandelier A, André F, Laurent F. Detection of *Chalara fraxinea* in common ash (*Fraxinus excelsior*) using real time PCR. *For Pathol* 2010;**40**:87–95.

Chandelier A, Helson M, Dvorak M *et al.* Detection and quantification of airborne inoculum of *Hymenoscyphus pseudoalbidus* using real-time PCR assays. *Plant Pathol* 2014;**63**:1296–305.

Chung Y, Rabe-Hesketh S, Dorie V *et al.* A Nondegenerate Penalized Likelihood Estimator for Variance Parameters in Multilevel Models. *Psychometrika* 2013;**78**:685–709.

Clark CJ, Poulsen JR, Bolker BM *et al.* Comparative seed shadows of bird-, monkey-, and wind-dispersed trees. *Ecology* 2005;**86**:2684–94.

Clark JS, Silman M, Kern R *et al.* Seed dispersal near and far: patterns across temperate and tropical forests. *Ecology* 1999;**80**:1475–94.

Crous PW, Groenewald JZ. Hosts, species and genotypes: opinions versus data. *Australas Plant Pathol* 2005;**34**:463.

Cunniffe NJ, Cobb RC, Meentemeyer RK *et al.* Modeling when, where, and how to manage a forest epidemic, motivated by sudden oak death in California. *Proc Natl Acad Sci* 2016;**113**:5640–5.

Desprez-Loustau M-L, Aguayo J, Dutech C *et al.* An evolutionary ecology perspective to address forest pathology challenges of today and tomorrow. *Ann For Sci* 2016;**73**:45–67.

Devaux C, Lavigne C, Austerlitz F *et al.* Modelling and estimating pollen movement in oilseed rape (*Brassica napus*) at the landscape scale using genetic markers: Landscape oilseed rape pollination. *Mol Ecol* 2006;**16**:487–99.

Dvorak M, Rotkova G, Botella L. Detection of Airborne Inoculum of *Hymenoscyphus fraxineus* and *H. albidus* during Seasonal Fluctuations Associated with Absence of Apothecia. *Forests* 2016;**7**:1.

Edman M, Gustafsson M. Wood-disk traps providea robust method for studying spore dispersal of wood-decaying basidiomycetes. *Mycologia* 2003;**95**:553–6.

Gonthier P, Garbelotto M, Varese GC *et al.* Relative abundance and potential dispersal range of intersterility groups of *Heterobasidion annosum* in pure and mixed forests. *Can J Bot* 2001;**79**:1057–65.

Grosdidier M, Aguayo J, Marçais B *et al.* Detection of plant pathogens using real-time PCR: how reliable are late Ct values? *Plant Pathol* 2017;**66**:359–67.

Gross A. Reproduction system and population structure of *Hymenoscyphus pseudoalbidus*, causal agent of ash dieback. 2013.

Gross A, Holdenrieder O, Pautasso M *et al. Hymenoscyphus pseudoalbidus*, the causal agent of European ash dieback: *H. pseudoalbidus*, the causal agent of ash dieback. *Mol Plant Pathol* 2014;**15**:5–21.

Gross A, Zaffarano PL, Duo A *et al.* Reproductive mode and life cycle of the ash dieback pathogen *Hymenoscyphus pseudoalbidus*. *Fungal Genet Biol* 2012;**49**:977–86.

Hauptman T, Piškur B, de Groot M *et al.* Temperature effect on *Chalara fraxinea* : heat treatment of saplings as a possible disease control method. Holdenrieder O (ed.). *For Pathol* 2013;**43**:360–70.

Hietala AM, Timmermann V, BØrja I *et al.* The invasive ash dieback pathogen *Hymenoscyphus pseudoalbidus* exerts maximal infection pressure prior to the onset of host leaf senescence. *Fungal Ecol* 2013;**6**:302–8.

Husson C, Scala B, Caël O *et al. Chalara fraxinea* is an invasive pathogen in France. *Eur J Plant Pathol* 2011;**130**:311–24.

Ioos R, Fourrier C. Validation and accreditation of a duplex real-time PCR test for reliable in planta detection of *Chalara fraxinea*: Duplex RT-PCR for in planta detection of *C. fraxinea*. *EPPO Bull* 2011;**41**:21–6.

Ioos R, Fourrier C, Iancu G *et al.* Sensitive detection of *Fusarium circinatum* in pine seed by combining an enrichment procedure with a real-time polymerase chain reaction using dual-labeled probe chemistry. *Phytopathology* 2009a;**99**:582–590.

Ioos R, Kowalski T, Husson C *et al.* Rapid in planta detection of *Chalara fraxinea* by a real-time PCR assay using a dual-labelled probe. *Eur J Plant Pathol* 2009b;**125**:329–35.

Jackson SL, Bayliss KL. Spore traps need improvement to fulfil plant biosecurity requirements: Spore traps for biosecurity. *Plant Pathol* 2011;**60**:801–10.

Kowalski T. *Chalara fraxinea* sp. nov. associated with dieback of ash (*Fraxinus excelsior*) in Poland. *For Pathol* 2006;**36**:264–70.

Kowalski T, Bartnik C. Morphologial variation in colonies of *Chalara fraxinea* isolated from ash (*Fraxinus excelsior* L.) stems with symptoms of dieback and effects of temperature on colony growth and structure. *Acta Agrobot* 2012;**63**:99–106.

Laiviņš M, Priede A, Pušpure I. Spread of *Hymenoscyphus fraxineus* in Latvia: Analysis based on Dynamics of Young Ash Stands. *Proc Latv Acad Sci Sect B Nat Exact Appl Sci* 2016;**70**, DOI: 10.1515/prolas-2016-0020.

Luchi N, Ghelardini L, Belbahri L *et al.* Rapid Detection of *Ceratocystis platani* Inoculum by Quantitative Real-Time PCR Assay. *Appl Environ Microbiol* 2013;**79**:5394–404.

Mahaffee WF, Stoll R. The Ebb and Flow of Airborne Pathogens: Monitoring and Use in Disease Management Decisions. *Phytopathology* 2016;**106**:420–31.

McCracken AR, Douglas GC, Ryan C *et al.* Ash dieback on the island of Ireland. *Dieback of European Ash (*Fraxinus *Spp.)*. Uppsala: Swedish University of Agricultural Sciences, 2017, 125.

Meentemeyer RK, Cunniffe NJ, Cook AR *et al.* Epidemiological modeling of invasion in heterogeneous landscapes: spread of sudden oak death in California (1990–2030). *Ecosphere* 2011;**2**:art17.

Nageleisen L-M, Saintonge F-X, Piou D. *La Santé Des Forêts: Maladies, Insectes, Accidents Climatiques... Diagnostic et Prévention*. Forêt privée française, 2010.

Nathan R, Klein E, Robledo-Arnuncio JJ *et al.* Dispersal kernels: review. *Dispersal Ecol Evol Oxf Univ Press Oxf Pp* 2012:187–210.

Norros V, Rannik Ü, Hussein T *et al.* Do small spores disperse further than large spores? *Ecology* 2014;**95**:1612–21.

Pan Z, Yang XB, Pivonia S *et al.* Long-Term Prediction of Soybean Rust Entry into the Continental United States. *Plant Dis* 2006;**90**:840–6.

Peterson, E.K., Hansen, E.M., and Kanaskie, A. Temporal Epidemiology of Sudden Oak Death in Oregon. *Phytopathology* 2015,105,937–946.

van Putten B, Visser MD, Muller-Landau HC *et al.* Distorted-distance models for directional dispersal: a general framework with application to a wind-dispersed tree: Distorted-distance models for directional dispersal. *Methods Ecol Evol* 2012;**3**:642–52.

Queloz V, Grünig CR, Berndt R *et al.* Cryptic speciation in *Hymenoscyphus albidus*: Speciation in *Hymenoscyphus albidus*. *For Pathol* 2011;**41**:133–42.

Rieux A, Soubeyrand S, Bonnot F *et al.* Long-Distance Wind-Dispersal of Spores in a Fungal Plant Pathogen: Estimation of Anisotropic Dispersal Kernels from an Extensive Field Experiment. Wilson RA (ed.). *PLoS ONE* 2014;**9**:e103225.

Santini A, Ghelardini L, De Pace C *et al.* Biogeographical patterns and determinants of invasion by forest pathogens in Europe. *New Phytol* 2013;**197**:238–50.

Scherm H. 1996. On the velocity of epidemic waves in model plant disease epidemics. *Ecological Modelling* **87**: 217-222.

Schurr FM, Steinitz O, Nathan R. Plant fecundity and seed dispersal in spatially heterogeneous environments: models, mechanisms and estimation. *J Ecol* 2008;**96**:628–41.

Schweigkofler W, O'Donnell K, Garbelotto M. Detection and Quantification of Airborne Conidia of Fusarium circinatum, the Causal Agent of Pine Pitch Canker, from Two California Sites by Using a Real-Time PCR Approach Combined with a Simple Spore Trapping Method. *Appl Environ Microbiol* 2004;**70**:3512–20.

Skovsgaard JP, Wilhelm GJ, Thomsen IM *et al.* Silvicultural strategies for *Fraxinus excelsior* in response to dieback caused by *Hymenoscyphus fraxineus*. *For Int J For Res* 2017:1–18.

Stansbury CD, McKirdy SJ, Diggle AJ *et al.* Modeling the Risk of Entry, Establishment, Spread, Containment, and Economic Impact of *Tilletia indica* , the Cause of Karnal Bunt of Wheat, Using an Australian Context. *Phytopathology* 2002;**92**:321–31.

Stenlid J, Oliva J, Boberg JB *et al.* Emerging Diseases in European Forest Ecosystems and Responses in Society. *Forests* 2011;**2**:486–504.

Timmermann V, Børja I, Hietala AM *et al.* Ash dieback: pathogen spread and diurnal patterns of ascospore dispersal, with special emphasis on Norway. *EPPO Bull* 2011;**41**:14–20.

Williams F, Eschen R, Harris A *et al.* The economic cost of invasive non-native species on Great Britain. *CABI Rep 198pp* 2010.